Title

Effect of halogen ions on low thermal conductivity of cesium halide perovskite

Author

Shoya Kawano 1

Terumasa Tadano 2

Satoshi Iikubo 1

1 Kyushu Institute of Technology, Kitakyushu, Fukuoka 8080196, Japan.

2 National Institute for Materials Science, Tsukuba, Ibaraki 3050047, Japan.

Keywords

Self-consistent phonon theory, first-principles calculation, halide perovskite, lattice thermal conductivity

Abstract

The lattice dynamics of $CsSnX_3$ (X = Cl, Br, and I) and $CsPbI_3$, which are low thermal conductivity materials, are investigated using first-principles phonon calculations. Because of the strong lattice anharmonicity and accompanying instability of high-temperature cubic phases, the self-consistent phonon theory, which can incorporate the effect of lattice anharmonicity at a mean-field level, is applied in this study. The calculated lattice thermal conductivity reproduced a low thermal conductivity, as shown experimentally, owing to the short phonon lifetime due to the incoherent scattering contribution of Cs atoms. The halogen ion dependence on thermal conductivity reveals that $CsSnCl_3$ exhibits an anomalous lattice thermal conductivity that is as low as that of $CsSnBr_3$. This indicates that the lattice dynamics cannot be explained merely in terms of the atomic mass of the compounds. The low thermal conductivity of $CsSnCl_3$ is caused by the exceptionally short phonon lifetime; further, a bonding analysis suggests that covalent bonding contributes significantly to the unusual anharmonicity of $CsSnCl_3$.

1. Introduction

The efficiency of a thermoelectric material can be estimated by a dimensionless figure of merit *ZT,* which is defined as $S^2\sigma T/\kappa$, where S is the Seebeck coefficient, σ is the electrical conductivity, T is the temperature, and κ is the thermal conductivity [1]. For a better conversion efficiency, the Seebeck coefficient and electrical conductivity must be increased, whereas the thermal conductivity must be reduced. Previous studies indicate that the formation of grain boundaries and interfaces in thermoelectric materials enhances phonon scattering, resulting in desirable thermal conductivities [2-4]. In addition, lattice thermal conductivity decreases with the increase in phonon scattering due to the rattling motion of embedded atoms. This mechanism is well known in clathrate or skutterudite compounds and has been suggested for cesium halide perovskite systems [5].

The general chemical formula of halide perovskites is ABX_3, where A represents organic molecule CH_3NH_3 or inorganic atom Cs, B represents Pb or Sn, and X represents halogen (I, Br, Cl) atoms [5-8]. These halide perovskites have been studied extensively as light absorbers for solar cells [9-11]. Pisoni *et al*. reported that $CH_3NH_3PbI_3$ has a low thermal conductivity (0.3–0.5 W/mK at 300 K) [12]. This thermal property suggests the potential of halide perovskites as a thermoelectric material. Furthermore, Lee *et al.* [5] reported the low lattice thermal conductivities of all-inorganic halide perovskites $CsSnI_3$ (orthorhombic), $CsPbBr_3$ (orthorhombic), and $CsPbI_3$ (yellow polymorph), which were 0.38, 0.42, and 0.45 W/mK at room temperature, respectively. These studies indicate that all-inorganic halide perovskites have ultralow lattice thermal conductivities.

Materials that have low thermal conductivities are expected to exhibit unique and interesting lattice dynamics. Except for the rattling mechanism, Hata *et al*. presented the mechanism contributing to the low thermal transport properties of $CH_3NH_3PbI_3$ [13]. They discovered that a decreasing thermal conductivity is mainly derived from the rotation motion of CH_3NH_3 molecules. Furthermore, Shulumba *et al*. reported the unusual low thermal conductivity of PbSe due to its unusual thermal conductivity arising from its intrinsic localized mode that halts thermal transport [14]. The intrinsic localized mode of PbSe is confirmed by neutron scattering measurements [15]. Rattling motions or the intrinsic localization mode are interesting and important for thermal transport as they reveal the details of phonon properties through calculations. In this regard, first-principles calculations are crucial for investigating the phonon properties of halide perovskites, regardless of whether

rattling motions and other contributions affect the lattice thermal conductivity.

However, in these low-lattice thermal conductivity materials, the phonon lifetime is reduced owing to phonon–phonon scattering, and this strong lattice anharmonicity leads to breakdown of simple picture, which approximates lattice vibration as a harmonic oscillator. Furthermore, halide perovskites are known to undergo a transition from the orthorhombic to tetragonal to cubic phase as a function of temperature [6, 16]. Although the lattice thermal conductivity of the cubic phase was evaluated by first-principles phonon calculation [7], their lattice thermal conductivity was affected by the phonon soft modes. Such dynamical instability has also been reported in a previous phonon study [17]. Hence, to estimate the lattice thermal conductivity of the high-temperature phase, self-consistent phonon (SCPH) theory is an appropriate approach, which includes lattice anharmonicity and enables us to calculate the accurate phonon frequency at a finite temperature. This approach was successfully employed for cubic $SrTiO_3$ perovskite, which is of a high-temperature phase [18]. Patrick *et al*. reported the phonon dispersion of cubic $CsSnI_3$ at 500 K using SCPH theory [19]. Furthermore, using SCPH theory, the lattice thermal conductivity of cubic perovskites can be calculated.

Herein, we report the lattice dynamics of all-inorganic halide perovskites of cubic $CsSnX_3$ (X = Cl, Br, and I) and $CsPbI_3$ using SCPH theory. SCPH theory successfully reproduces the phonon dispersion of the finite temperature, which is consistent with a previous study [19]. The lattice thermal conductivity of cubic phases based on the Boltzmann transport equation within the relaxation time approximation shows the unusual lattice thermal conductivity of $CsSnCl_3$. This is related to the short phonon lifetime caused by the difference in covalent bonding. This study is the first to provide the thermal properties of cubic all-inorganic halide perovskites $CsSnX_3$ (X = Cl, Br, and I) and $CsPbI_3$ based on first-principles calculations.

2. Calculation procedure

We performed first-principles phonon calculations for cubic $CsSnX_3$ (X = Cl, Br, and I) and $CsPbI_3$ using the self-consistent phonon approach implemented in the ALAMODE code [18, 20] with VASP code [21-22]. The simplest approximation in lattice dynamics theory is harmonic approximation. By considering the potential energy V between two atoms, we can express energy as a Taylor expansion with respect to atomic displacements from equilibrium positions at zero temperature:

$$V - V_0 = V_2 + V_3 + V_4 + \cdots = \frac{1}{2!}\sum_{i,j}\Phi_{i,j}u_i u_j + \frac{1}{3!}\sum_{i,j,k}\Phi_{i,j,k}u_i u_j u_k + \frac{1}{4!}\sum_{i,j,k,l}\Phi_{i,j,k,l}u_i u_j u_k u_l + \cdots, \quad (1)$$

where V_n is the potential energy of the nth-order contribution, Φ is the force constant, and u is the atomic displacement with the index of atoms i, j, k, and l. The harmonic approximation involves neglecting all terms of power higher than two. The harmonic approximation provides many features, such as a link between vibrational frequencies, wave vectors, and interatomic forces, and applications in areas such as the thermodynamic properties of materials. Meanwhile, several physical properties, such as thermal expansion and thermal conductivity, and behaviors such as phase transitions, are not explained by the harmonic model. These properties originate from lattice anharmonicity and can be treated theoretically by including higher-order terms.

The second- and fourth-order force constants should be extracted to calculate the phonon dispersion, including the anharmonic effect with SCPH theory [18]. The anharmonic phonon frequency Ω is defined as follows:

$$\Omega_q{}^2 = \omega_q{}^2 + 2\Omega_q I_q, \quad (2)$$

where ω_q is the harmonic phonon frequency calculated by second-order force constants, and I_q is the anharmonic phonon self-energy calculated by fourth-order force constants. First, we calculated the phonon dispersion only with second-order force constants. Next, by solving this equation self-consistently, we can obtain the anharmonic frequency Ω_q.

The third-order force constant is necessitated to evaluate the lattice thermal conductivity. In the Boltzmann transport equation within the relaxation time approximation, the lattice conductivity is expressed as the product of the specific heat c, phonon group velocity v, and lifetime τ. Here, the lattice thermal conductivity κ_{ph} is expressed as follows:

$$\kappa_{ph} = \frac{1}{NV}\sum_{q} c_q \, v_q^2 \tau_q, \tag{3}$$

where N is the number of q points in the Brillouin zone, and V is the volume of the cell. The specific heat and phonon group velocity can be calculated from the phonon dispersion. The phonon lifetime is calculated by the phonon scattering probability, which is derived from the third-order force constant. Therefore, we calculated the second-, third-, and fourth-order force constants from first-principles calculations. In this study, the fourth-order force constants were determined with fifth-nearest neighbor shells, whereas fifth-and sixth-order force constants were considered for fifth-nearest neighbor pairs. These force constants were extracted from displacement–force datasets using the linear regression implemented in ALAMODE. We examined two displacement–force datasets. One is the finite displacement (FD) dataset [23-24], another is the first-principles molecular dynamics (FPMD) dataset [25-26].

In the DFT calculation, the interaction between the ion core and valence electrons was described by the projector-augmented wave method [27-28]. The exchange and correlation functions were obtained using a generalized gradient approximation, as proposed by Perdew *et al.* [29-30]. We used a plane wave energy cutoff of 400 eV, a convergence criterion for the electronic self-consistency loop of 10^{-8} eV, a Γ-point-centered k-mesh that was limited to 0.15 $Å^{-1}$, and the Gaussian smearing method with a smearing width of 0.05 eV. We calculated the Born effective charges and the dielectric tensor using density functional perturbation theory to consider the nonanalytic part of the dynamical matrix. For the finite displacement approach, we used a displacement distance of 0.01 Å. For FPMD, we used the 2000 step results without the initial 1000 steps simulated at T = 300 K with a timestep of 1 fs. These results provided the 2000 atomic configuration for FPMD dataset, but the displacement at only T = 300 K is not suitable for calculating temperature dependence of physical properties of systems. Therefore, additional data, where random displacements by 0.1 Å of 400 atomic

configurations equally spaced in time was added to FPMD dataset. This procedure follows previous studies [18, 31]. In addition, the least absolute shrinkage and selection operator (LASSO) technique was employed to estimate force constants. The hyperparameter of LASSO was selected by minimizing the four-fold cross-validation score.

3. Results & discussion

First, we calculated and compared the phonon dispersion of cubic $CsSnI_3$ using various calculation methods. The crystal structure of the cubic phase of the calculated halide perovskite ABX_3 was categorized as $Pm\bar{3}m$ (221). The *A*, *B*, and *X* atoms were located at the 1a, 1b, and 3d Wyckoff positions, respectively. The lattice constants of $CsSnI_3$ were a = 6.281 Å, which is similar to the experimental values of a = 6.2057 Å [32]. Figure 1 shows a comparison of the phonon dispersion calculated using various calculation methods. Dotted lines represent the calculated result of the harmonic approximation with second-order force constants in Eq. (1). The wave vectors of the phonon dispersion are shown along the high-symmetry points, Γ (0, 0, 0) - X (0.5, 0, 0) - M (0.5, 0.5, 0) - Γ (0, 0, 0) - R (0.5, 0.5, 0.5) - M (0.5, 0.5, 0). In this dispersion curve, a negative frequency was observed at the M and R points, which means that cubic $CsSnI_3$ is dynamically unstable at T = 0. This result is consistent with those of the previous studies [7, 17, 19].

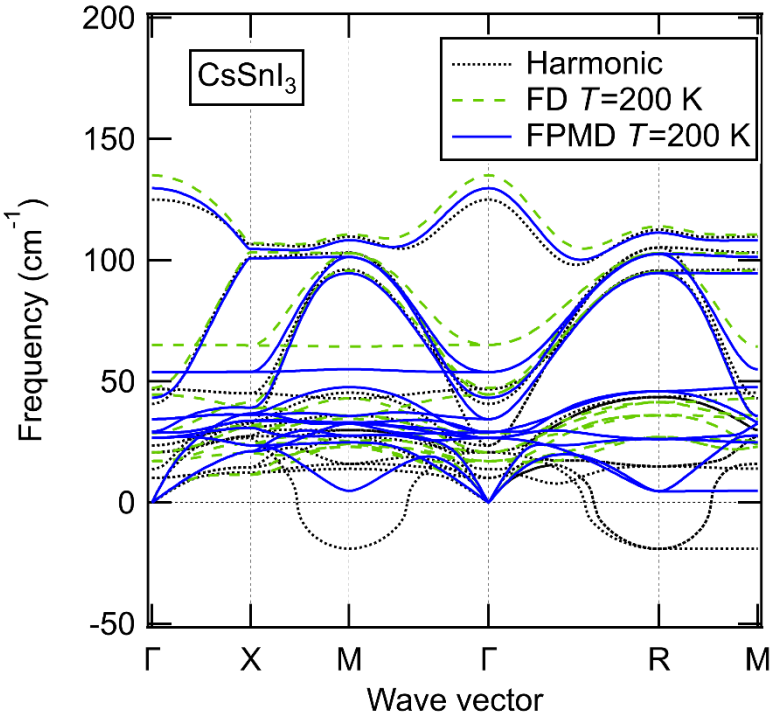

Fig. 1 Phonon dispersion of cubic $CsSnI_3$ calculated using harmonic approximations (dotted lines) and SCPH theory at 200 K. Solid and dashed lines show results with force constants extracted using FPMD and FD methods, respectively.

For the high-temperature stable phase, the SCPH calculation enables us to obtain the phonon dispersion at a finite temperature by incorporating both the fourth- and second-order force constants. The solid and dashed lines show the results of the SCPH calculation. We analyzed three datasets to extract the fourth-order force constants: the FPMD with/without random displacements and FD datasets. For the FPMD dataset, the calculation converged at 140 K < T < 1000 K, where the convergence criteria included the positive phonon frequency. Convergence at a finite temperature in the SCPH calculation is a reasonable result in terms of lattice dynamics. Difference of the result between with and without the random displacement was quite small, hence the result of FPMD dataset with the random displacements is shown in this paper. However, for the FD dataset, the calculation converged at 0 < T < 220 K, which is rather unusual. The dispersion curves obtained were

compared at 200 K, where both SCPH calculations converged. A significantly difference was observed at points M and R. The cubic phase was experimentally reported as a stable phase above 440 K [6]. The result of the FPMD dataset, which was reproduced as a high-temperature stable phase, was consistent with experimental observations. Previous calculations indicated the phonon dispersion of cubic $CsSnI_3$ at 500 K [19], which is similar to our FPMD dataset dispersion at 500 K. In FD approach, we speculated that the displacement is too small to extract the high-order force constant, which is smaller effect than second- and third-order term. Therefore, the FPMD dataset with random displacement is preferred for extracting the fourth-order force constant in this study.

Figure 2 shows the phonon dispersions of $CsSnCl_3$, $CsSnBr_3$, and $CsPbI_3$ using SCPH theory at 300 K, which are compared with the result of harmonic approximation. The lattice constants of $CsSnX_3$ (X = Cl, and Br) and $CsPbI_3$ were a = 5.631, 5.895, and 6.395 Å, respectively, which were consistent with the experimental values ($CsSnCl_3$ a = 5.5734 Å; $CsSnBr_3$ a = 5.791 Å; $CsPbI_3$ a = 6.2894 Å) [32]. Solid and dotted lines show the results of SCPH theory at 300 K and harmonic approximation, respectively. Each halide perovskite contained no imaginary phonon mode owing to SCPH theory.

For the calculation temperature range $0 < T < 1000$ K at every 10 K step, self-consistent calculations converged at 80–1000 K for $CsSnCl_3$, 100–1000 K for $CsSnBr_3$, and 220–1000 K for $CsPbI_3$, indicating the absence of imaginary frequency and the stability for these temperature ranges. These results are consistent with the experimental observation, i.e., the cubic phase is a high-temperature phase. The experimental phase transition temperatures of the cubic phases of $CsSnCl_3$, $CsSnBr_3$, $CsSnI_3$, and $CsPbI_3$ were T = 293, 286, 440.5, and 634 K, respectively, [6, 33-35]. For the phase transition temperature, taking account of only fourth-order contribution for temperature dependence of phonon frequency was not enough for comparison with experimental values. We need to include the frequency shift or the thermal expansion effect from third-order anharmonic contribution. Furthermore, experimental observation suggested that the phase transitions in $CsPbI_3$ is not simple second-order phase transition[34].

The phonon dispersion of $CsPbI_3$ was distributed at lower frequencies compared with those of other perovskites. The distribution of phonon frequencies was simply understood in terms of the atomic mass of the compounds. The phonon dispersion and density of states indicated that the phonon frequency decreased with increasing atomic mass. Hence,

we can expect a low group velocity v ($v_q = \frac{\partial \omega_q}{\partial \boldsymbol{q}}$) for a heavy atomic mass system.

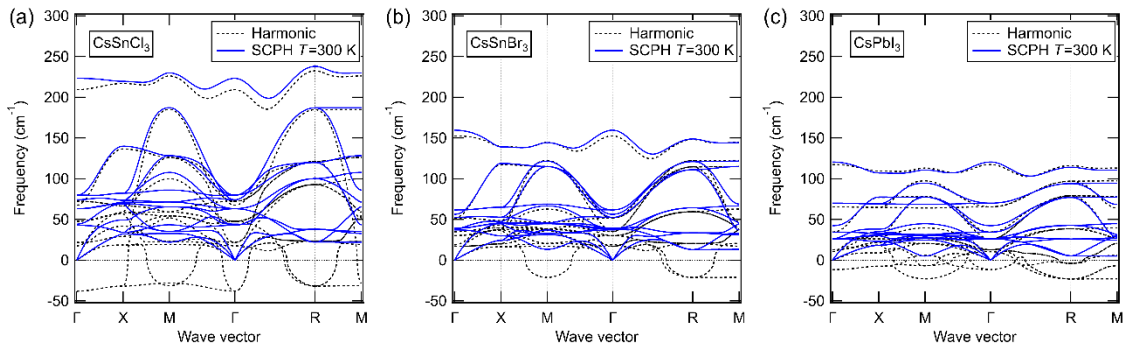

Fig. 2 Phonon dispersion of (a) $CsSnCl_3$, (b) $CsSnBr_3$, and (c) $CsPbI_3$. Solid lines show phonon dispersion at 300 K using SCPH method. Dotted lines show phonon dispersion within harmonic approximation.

The lattice thermal conductivity was calculated from the obtained phonon dispersions with no imaginary frequency. Figure 3 shows the lattice thermal conductivity of $CsSnX_3$ (X = Cl, Br, and I) and $CsPbI_3$. It is noteworthy that our calculations demonstrated the low lattice thermal conductivity in these halide perovskites. $CsPbI_3$ showed the lowest lattice thermal conductivity. This can be understood from the heavy atomic mass of Pb; a system with heavy atoms has a low group velocity owing to the low phonon frequency. Therefore, the highest lattice thermal conductivity of $CsSnCl_3$ was expected because of the lightweightness of Cl; however, the thermal conductivity of $CsSnCl_3$ is similar to that of $CsSnBr_3$. Compared with other Sn-based perovskites, the low lattice thermal conductivity of $CsSnCl_3$ appears unusual.

In a previous study [5], the lattice thermal conductivities of nano single crystals of $CsSnI_3$ (orthorhombic), $CsPbBr_3$ (orthorhombic), and $CsPbI_3$ (yellow polymorph) were reported to be κ_{ph} = 0.38, 0.42, and 0.45 W/mK at room temperature, respectively. Therefore, the halide perovskites indicated lower thermal conductivities than the calculated values. The difference between the calculated and experimental values may be due to the following reasons: (1) difference in crystal structure; (2) lattice imperfection not included in the calculation; (3) thermal expansion and high-order anharmonicity not included in the

calculation. We may be able to estimate the effect of thermal expansion and high-order anharmonicity; however, we would require the experimental data of high-quality bulk single crystals of cubic all-inorganic halide perovskites to disregard the effects of (1) and (2).

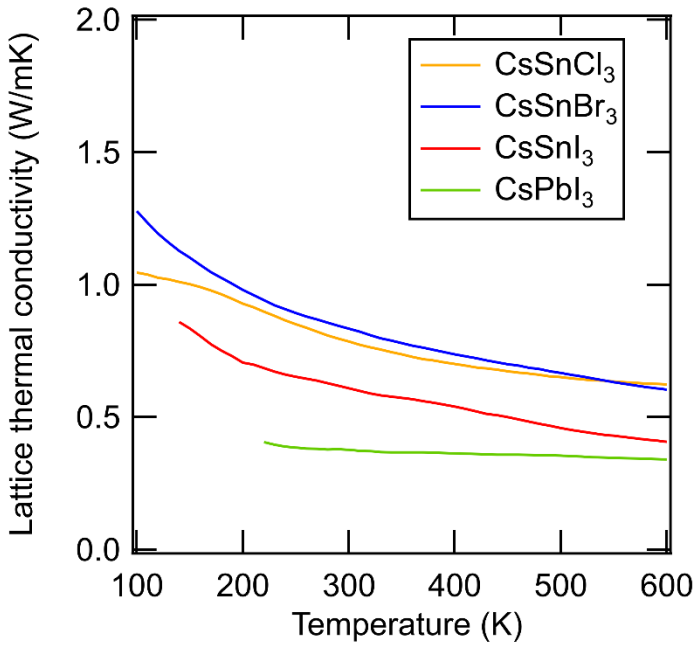

Fig. 3 Temperature dependence of lattice thermal conductivity of $CsSnX_3$ (X = Cl, Br, and I) and $CsPbI_3$.

The lattice thermal conductivity of $CsSnCl_3$ was low because the lattice thermal conductivity was proportional to the product of the specific heat, group velocity, and phonon lifetime. Figure 4(a) shows the frequency dependence of the group velocity at T = 300 K. The order of the group velocity was $CsPbI_3 < CsSnI_3 < CsSnBr_3 < CsSnCl_3$, which is clearly related to the order of atomic mass of the compounds. In $CsSnCl_3$, a high group velocity was observed in the frequency range of f = 100–200 cm^{-1}. Figure 4(b) shows the frequency dependence of the phonon lifetime at 300 K. We discovered that $CsSnCl_3$ exhibited a short phonon lifetime. The lifetime was shorter than that of the other perovskites above f = 100 cm^{-1}. The phonon lifetimes of $CsPbI_3$, $CsSnI_3$, and $CsSnBr_3$ indicate no clear differences, such as in the $CsSnCl_3$ case. Therefore, the phonon group velocity and lifetime indicate that $CsSnCl_3$ has a higher group velocity and shorter lifetime than the other perovskites.

In this study, the $CsPbI_3$ results were compared with those of previous neutron

scattering measurements for $CH_3NH_3PbI_3$ [36]. The phonon group velocity and lifetime of acoustic phonons in the experiment were reported to be v = 2400 or 1200 m/s and τ = 1–20 ps, respectively. Our data indicated v < 3000 m/s and $\tau \approx$ 1–40 ps for lower frequencies, which are similar to the results of the abovementioned experimental study, although the A site differed. Therefore, these phonon properties have been well described in our calculations. Additionally, we compared our phonon lifetimes with those of other materials. Our calculated lifetimes were one order of magnitude shorter than that of Si [37], two orders of magnitude shorter than those of GaAs and CdTe [38], and similar in magnitude to those of PbSe and PbTe [39]. From these comparisons, it was clear the phonon lifetime of the calculated halide perovskite was shorter than those of other materials.

Next, the frequency dependence of the spectrum-decomposed lattice thermal conductivities of $CsSnX_3$ (X = Cl, Br, and I) and $CsPbI_3$ at 300 K is shown in Fig. 4(c) to reveal the contribution of the phonon group velocity and lifetime to the lattice thermal conductivity. These spectra indicate that the lattice thermal conductivity was high around the peak frequency of the group velocity except for $CsSnCl_3$. Hence, the trend of the lattice thermal conductivities of $CsSnBr_3$, $CsSnI_3$, and $CsPbI_3$ were mainly determined by the phonon group velocity. However, $CsSnCl_3$ indicated a low lattice thermal conductivity around the peak frequency of the group velocity owing to the short lifetime around this frequency range. This indicates that the phonon lifetime contributed significantly to the lattice thermal conductivity of $CsSnCl_3$. We conclude that the low thermal conductivity of $CsSnCl_3$ was caused by the short phonon lifetime, which contributed more compared with the group velocity.

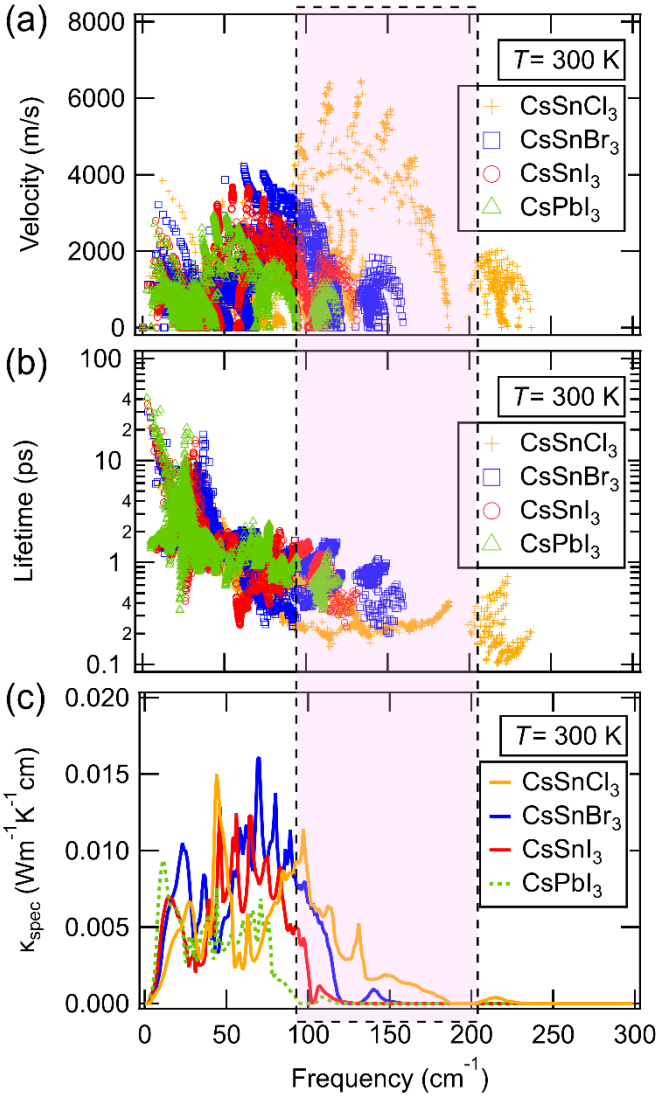

Fig. 4 Frequency dependence of (a) phonon group velocity, (b) phonon lifetime, and (c) spectrum-decomposed lattice thermal conductivity of $CsSnX_3$ (X = Cl, Br, and I) and $CsPbI_3$ at 300 K.

Next, we discuss the origin of the short phonon lifetime above f = 100 cm^{-1} for $CsSnCl_3$. The intrinsic localized mode reported in [14] is an interesting scenario for the anomalous behavior; however, it may be rejected in $CsSnCl_3$. From the phonon dispersions, as shown in Fig. 2, a flattening band was observed for all systems and not only for $CsSnCl_3$. Additionally, the rattling motion of Cs atoms was analyzed [5-6, 18]. The atom-projected phonon densities of states of $CsSnX_3$ (X = Cl, Br, and I) and $CsPbI_3$ are shown in Fig. 5. The phonon density of states of Cs atoms was distributed around 30 cm^{-1}. The distribution of Sn shifted to a higher frequency with increasing light atoms. Furthermore, the X site shifted to a high frequency with such a substitution. Although the rattling motion decreased the lattice thermal conductivity, it did not contribute to the short lifetime of $CsSnCl_3$ because the short lifetime was mainly observed above f = 100 cm^{-1}. However, Cs rattling motions causing a low thermal conductivity is expected for all Cs halide perovskite systems. Based on the phonon density of states and the dispersions, the flattening phonon mode as the intrinsic localized mode and the rattling of Cs atoms did not contribute to the unusual short lifetime of $CsSnCl_3$.

Meanwhile, we discovered that the phonon contribution above f = 100 cm^{-1} mainly comprised Sn and halide ions, as shown in Fig. 5. Sn and halogen ions were covalently bonded and adjacent to each other in the perovskite structure. We speculate that this covalent bonding may generate an anisotropic motion (vibration) of ions and cause a strong lattice anharmonicity in the system. To investigate this effect on the phonon lifetime, we conducted a bonding analysis of the Sn–X bonds for $CsSnX_3$. For chemical bond analysis, we calculated the projected crystal orbital Hamilton population (pCOHP) from the obtained DFT output using the local-orbital basis suite toward electronic-structure reconstruction code [40-43]. The pCOHP indicates the orbital-pair interaction (bonding, antibonding, or nonbonding) by estimating the overlap of the orbitals, which is analyzed from the wave function.

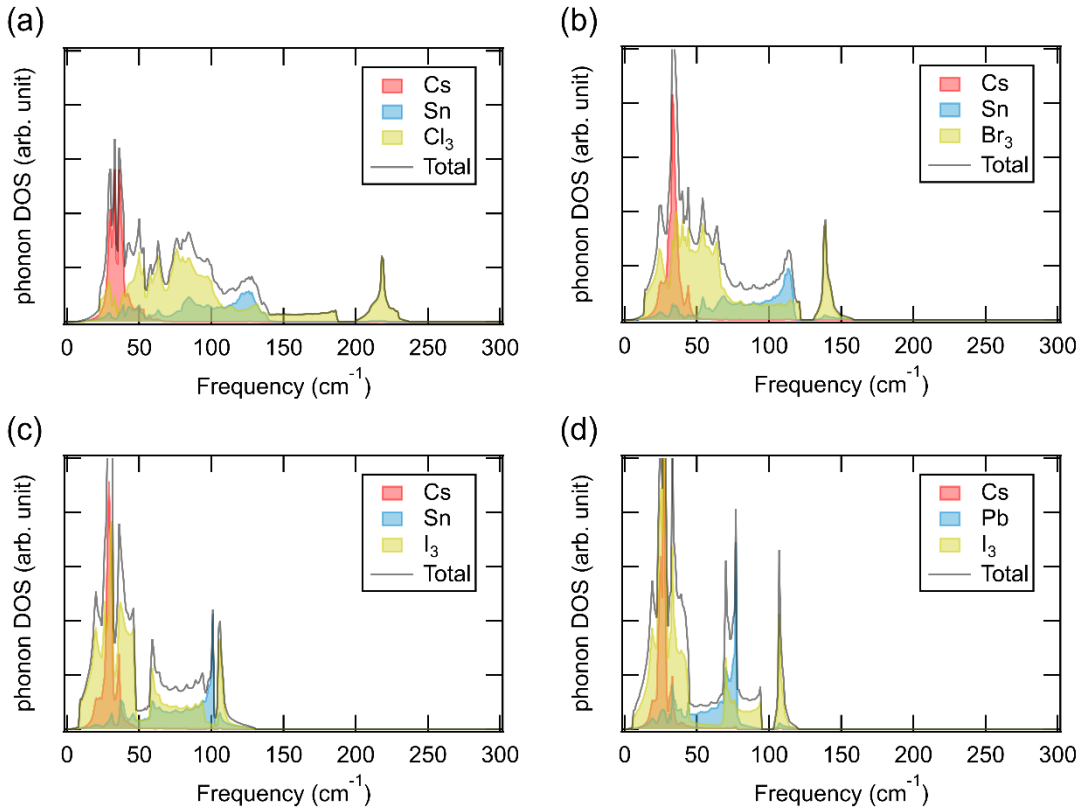

Fig. 5 Atom-projected phonon density of states of $CsSnX_3$ (X = Cl, Br, and I) and $CsPbI_3$.

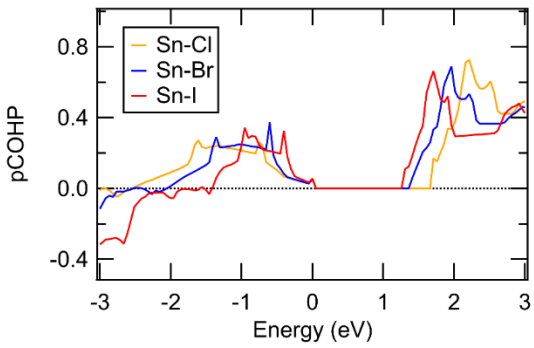

Fig. 6 Projected crystal orbital Hamilton populations of Sn–X (X = Cl, Br, I) bonds, where the energy is shown with respect to the Fermi energy.

Figure 6 shows the pCOHPs of Sn–X (X = Cl, Br, I) bonds, where the energy ε is shown with respect to the Fermi energy. The pCOHP indicates the antibonding contribution by a positive sign, such that the Sn–X bonds around the bandgap are antibonding contributions. This bonding interaction for Sn–I is similar to those for $MASnI_3$ and $FASnI_3$ [44]. We focused on the occupied region ($\varepsilon < 0$). For the X = Cl case, the population ($-2.5 < \varepsilon < 0$) was broader than that of the X = I case ($-1.5 < \varepsilon < 0$). The overlap of orbitals between Sn–Cl and Sn–I bonding differed. A broad pCOHP in $CsSnCl_3$ implies a large transfer integral between the Sn and Cl orbitals; therefore, a strong covalent bond is expected in Sn–Cl bonding. This calculated result is consistent with our speculation. Whereas the pCOHP analysis presents the chemical bonding information for covalent bonding, such an overlap difference indicates the difference in covalent bonding between Sn–Cl and other pairs. Hence, we speculate that the unusual lattice anharmonicity of $CsSnCl_3$ was caused by the difference in covalent bonding.

4. Conclusion

We investigated the lattice dynamics and lattice thermal conductivity of the cubic phases of $CsSnX_3$ (X = Cl, Br, and I) and $CsPbI_3$ halide perovskites using first-principles phonon calculations based on the SCPH theory. From the phonon dispersion at a finite temperature, we discovered that the cubic phase was metastable. The lattice thermal conductivity of cubic halide perovskites was calculated using the Boltzmann transport equation with a relaxation time approximation. The calculated lattice thermal conductivities of cubic halide perovskites indicated a low thermal conductivity, which was slightly larger than the experimental value at low-temperature phases. We discovered that $CsSnCl_3$ exhibited an anomalously low lattice thermal conductivity because of its short phonon lifetime. Our analysis indicated that Sn and Cl were contributed around the frequency range of short phonon lifetime. Based on the phonon density of states and dispersions, clear evidence of participation of the rattling motion or the flattening phonon mode did not observed as the origin of the unusual short lifetime. Instead, we speculated based on bonding analysis that the unusual anharmonicity of $CsSnCl_3$ was caused by the difference in covalent bonding. Present calculation techniques are useful for obtaining the thermal properties of all-inorganic halide perovskites at high-temperature phases. Our approach incorporating SCPH theory provides a new perspective on anharmonic materials.

Acknowledgement

This study was supported by JST CREST (Grant No. JPMJCR17I4), Japan.

References

(1) Hicks, L. D.; Dresselhaus, M. S., Effect of quantum-well structures on the thermoelectric figure of merit. *Phys. Rev. B* **1993**, *47*, 12727-12731.

(2) Ge, Z.-H.; Zhao, L.-D.; Wu, D.; Liu, X.; Zhang, B.-P.; Li, J.-F.; He, J., Low-cost, abundant binary sulfides as promising thermoelectric materials. *Mater. Today* **2016**, *19*, 227-239.

(3) Li, J. M.; Li, D.; Song, C. J.; Wang, L.; Xin, H. X.; Zhang, J.; Qin, X. Y., Realized high power factor and thermoelectric performance in Cu_3SbSe_4. *Intermetallics* **2019**, *109*, 68-73.

(4) Shang, H.-J.; Ding, F.-Z.; Deng, Y.; Zhang, H.; Dong, Z.-B.; Xu, W.-J.; Huang, D.-X.; Gu, H.-W.; Chen, Z.-G., Highly (00l)-oriented Bi_2Te_3/Te heterostructure thin films with enhanced power factor. *Nanoscale* **2018**, *10*, 20189-20195.

(5) Lee, W., et al., Ultralow thermal conductivity in all-inorganic halide perovskites. *Proc. Natl. Acad. Sci. USA* **2017**, *114*, 8693-8697.

(6) Chung, I.; Song, J. H.; Im, J.; Androulakis, J.; Malliakas, C. D.; Li, H.; Freeman, A. J.; Kenney, J. T.; Kanatzidis, M. G., $CsSnI_3$: Semiconductor or metal? High electrical conductivity and strong near-infrared photoluminescence from a single material. High hole mobility and phase-transitions. *J. Am. Chem. Soc.* **2012**, *134*, 8579-87.

(7) Guo, S.-D.; Wang, J.-L., Potential thermoelectric materials $CsMI_3$ (M = Sn and Pb) in perovskite structures from first-principles calculations. *RSC Advances* **2016**, *6*, 101552-101559.

(8) Jena, A. K.; Kulkarni, A.; Miyasaka, T., Halide perovskite photovoltaics: Background, status, and future prospects. *Chem. Rev.* **2019**, *119*, 3036-3103.

(9) Kojima, A.; Teshima, K.; Shirai, Y.; Miyasaka, T., Organometal halide perovskites as visible-light sensitizers for photovoltaic cells. *J. Am. Chem. Soc.* **2009**, *131*, 6050-6051.

(10) Yamamoto, K.; Iikubo, S.; Yamasaki, J.; Ogomi, Y.; Hayase, S., Structural stability of iodide perovskite: A combined cluster expansion method and first-principles study. *J. Phys. Chem. C* **2017**, *121*, 27797-27804.

(11) Ito, N.; Kamarudin, M. A.; Hirotani, D.; Zhang, Y.; Shen, Q.; Ogomi, Y.; Iikubo, S.; Minemoto, T.; Yoshino, K.; Hayase, S., Mixed Sn-Ge perovskite for enhanced perovskite solar cell performance in air. *J. Phys. Chem. Lett.* **2018**, *9*, 1682-1688.

(12) Pisoni, A.; Jacimovic, J.; Barisic, O. S.; Spina, M.; Gaal, R.; Forro, L.; Horvath, E., Ultra-low thermal conductivity in organic-inorganic hybrid perovskite $CH_3NH_3PbI_3$. *J. Phys.*

Chem. Lett. **2014**, *5*, 2488-92.
(13) Hata, T.; Giorgi, G.; Yamashita, K., The effects of the organic-inorganic interactions on the thermal transport properties of $CH_3NH_3PbI_3$. *Nano Lett.* **2016**, *16*, 2749-53.
(14) Shulumba, N.; Hellman, O.; Minnich, A. J., Intrinsic localized mode and low thermal conductivity of PbSe. *Phys. Rev. B* **2017**, *95*.
(15) Manley, M. E., et al., Intrinsic anharmonic localization in thermoelectric PbSe. *Nat Commun* **2019**, *10*, 1928.
(16) Huang, L.-y.; Lambrecht, W. R. L., First-principles calculations of phonons and Raman spectra in monoclinic $CsSnCl_3$. *Phys. Rev. B* **2015**, *91*.
(17) Huang, L.-y.; Lambrecht, W. R. L., Lattice dynamics in perovskite halides $CsSnX_3$ with X=I, Br, Cl. *Phys. Rev. B* **2014**, *90*.
(18) Tadano, T.; Tsuneyuki, S., Self-consistent phonon calculations of lattice dynamical properties in cubic $SrTiO_3$ with first-principles anharmonic force constants. *Phys. Rev. B* **2015**, *92*, 054301.
(19) Patrick, C. E.; Jacobsen, K. W.; Thygesen, K. S., Anharmonic stabilization and band gap renormalization in the perovskite $CsSnI_3$. *Phys. Rev. B* **2015**, *92*.
(20) Tadano, T.; Gohda, Y.; Tsuneyuki, S., Anharmonic force constants extracted from first-principles molecular dynamics: applications to heat transfer simulations. *J. Phys. Condens. Matter.* **2014**, *26*, 225402.
(21) Kresse, G.; Furthmüller, J., Efficiency of ab-initio total energy calculations for metals and semiconductors using a plane-wave basis set. *Comp. Mater. Sci.* **1996**, *6*, 15-50.
(22) Kresse, G.; Furthmuller, J., Efficient iterative schemes for ab initio total-energy calculations using a plane-wave basis set. *Phys. Rev. B* **1996**, *54*, 11169-11186.
(23) Kresse, G.; Furthmüller, J.; Hafner, J., Ab initio force constant approach to phonon dispersion relations of diamond and graphite. *Europhys. Lett.* **1995**, *32*, 729.
(24) Parlinski, K.; Li, Z. Q.; Kawazoe, Y., First-principles eetermination of the soft mode in cubic ZrO_2. *Phys. Rev. Lett.* **1997**, *78*, 4063-4066.
(25) Esfarjani, K.; Stokes, H. T., Method to extract anharmonic force constants from first principles calculations. *Phys. Rev. B* **2008**, *77*.
(26) Esfarjani, K.; Stokes, H. T., Erratum: Method to extract anharmonic force constants from first principles calculations [Phys. Rev. B77, 144112 (2008)]. *Phys. Rev. B* **2012**, *86*.
(27) Blöchl, P. E., Projector augmented-wave method. *Phys. Rev. B* **1994**, *50*, 17953-17979.

(28) Kresse, G.; Joubert, D., From ultrasoft pseudopotentials to the projector augmented-wave method. *Phys. Rev. B* **1999**, *59*, 1758-1775.
(29) Perdew, J. P.; Burke, K.; Ernzerhof, M., Generalized gradient approximation made simple. *Phys. Rev. Lett.* **1996**, *77*, 3865-3868.
(30) Perdew, J. P.; Burke, K.; Ernzerhof, M., Erratum: Generalized gradient approximation made simple [Phys. Rev. Lett. 77, 3865 (1996)]. *Phys. Rev. Lett.* **1997**, *78*, 1396-1396.
(31) Zhou, F.; Nielson, W.; Xia, Y.; Ozolins, V., Lattice anharmonicity and thermal conductivity from compressive sensing of first-principles calculations. *Phys. Rev. Lett.* **2014**, *113*, 185501.
(32) Villars, P.; Cenzual, K., *Pearson's Crystal Data: Crystal Structure Database for Inorganic Compounds (on DVD), Release 2018/19*; ASM International®: Materials Park, Ohio, USA.
(33) Yang, R. X.; Skelton, J. M.; da Silva, E. L.; Frost, J. M.; Walsh, A., Spontaneous octahedral tilting in the cubic inorganic cesium halide perovskites $CsSnX_3$ and $CsPbX_3$ (X = F, Cl, Br, I). *J. Phys. Chem. Lett.* **2017**, *8*, 4720-4726.
(34) Trots, D. M.; Myagkota, S. V., High-temperature structural evolution of caesium and rubidium triiodoplumbates. *J. Phys. Chem. Solids* **2008**, *69*, 2520-2526.
(35) Fabini, D. H., et al., Dynamic stereochemical activity of the Sn^{2+} lone pair in perovskite $CsSnBr_3$. *J. Am. Chem. Soc.* **2016**, *138*, 11820-32.
(36) Gold-Parker, A.; Gehring, P. M.; Skelton, J. M.; Smith, I. C.; Parshall, D.; Frost, J. M.; Karunadasa, H. I.; Walsh, A.; Toney, M. F., Acoustic phonon lifetimes limit thermal transport in methylammonium lead iodide. *Proc. Natl. Acad. Sci. USA* **2018**, *115*, 11905-11910.
(37) Hellman, O.; Abrikosov, I. A., Temperature-dependent effective third-order interatomic force constants from first principles. *Phys. Rev. B* **2013**, *88*.
(38) Whalley, L. D.; Skelton, J. M.; Frost, J. M.; Walsh, A., Phonon anharmonicity, lifetimes, and thermal transport in $CH_3NH_3PbI_3$ from many-body perturbation theory. *Phys. Rev. B* **2016**, *94*.
(39) Tian, Z.; Garg, J.; Esfarjani, K.; Shiga, T.; Shiomi, J.; Chen, G., Phonon conduction in PbSe, PbTe, and $PbTe_{1-x}Se_x$ from first-principles calculations. *Phys. Rev. B* **2012**, *85*.
(40) Dronskowski, R.; Blöchl, P. E., Crystal orbital Hamilton populations (COHP): energy-resolved visualization of chemical bonding in solids based on density-functional

calculations. *J. Phys. Chem.* **1993**, *97*, 8617-8624.
(41) Deringer, V. L.; Tchougréeff, A. L.; Dronskowski, R., Crystal orbital Hamilton population (COHP) analysis as projected from plane-wave basis sets. *J. Phys. Chem. A* **2011**, *115*, 5461-5466.
(42) Maintz, S.; Deringer, V. L.; Tchougréeff, A. L.; Dronskowski, R., Analytic projection from plane-wave and PAW wavefunctions and application to chemical-bonding analysis in solids. *J. Comput. Chem.* **2013**, *34*, 2557-2567.
(43) Maintz, S.; Deringer, V. L.; Tchougréeff, A. L.; Dronskowski, R., LOBSTER: A tool to extract chemical bonding from plane‐wave based DFT. *J. Comput. Chem.* **2016**, *37*, 1030-1035.
(44) Shi, T.; Zhang, H.-S.; Meng, W.; Teng, Q.; Liu, M.; Yang, X.; Yan, Y.; Yip, H.-L.; Zhao, Y.-J., Effects of organic cations on the defect physics of tin halide perovskites. *J. Mater. Chem. A* **2017**, *5*, 15124-15129.

Table of contents